ACS APPLIED MATERIALS & INTERFACES

Research Article

www.acsami.org

Magnetically Aligned Iron Oxide/Gold Nanoparticle-Decorated Carbon Nanotube Hybrid Structure as a Humidity Sensor

Jaewook Lee,*[,†] Suresh Mulmi,[‡] Venkataraman Thangadurai,[‡] and Simon S. Park*[,†]

[†]Department of Mechanical and Manufacturing Engineering and [‡]Department of Chemistry, University of Calgary, Calgary, Alberta T2N 1N4, Canada

Supporting Information

ABSTRACT: Functionalized carbon nanotubes (f-CNTs), particularly CNTs decorated with nanoparticles (NPs), are of great interest because of their synergic effects, such as surface-enhanced Raman scattering, plasmonic resonance energy transfer, magnetoplasmonic, magnetoelectric, and magneto-optical effects. In general, research has focused on a single type of NP, such as a metal or metal oxide, that has been modified on a CNT surface. In this study, however, a new strategy is introduced for the decoration of two different NP types on CNTs. In order to improve the functionality of modified CNTs, we successfully prepared binary NP-decorated CNTs, namely, iron oxide/gold (Au) NP-decorated CNTs (IA-CNTs), which were created through two simple reactions in deionized water, without high temperature, high pressure, or harsh reducing agents. The physicochemical properties of IA-CNTs were characterized by ultraviolet/visible spectroscopy, Fourier transform infrared spectroscopy, a superconducting quantum interference device, scanning electron microscopy, and transmission electron microscopy. In this study, IA-CNTs were utilized to detect humidity. Magnetic IA-CNTs were aligned on interdigitated platinum electrodes under external magnetic fields to create a humidity-sensing channel, and its electrical conductivity was monitored. As the humidity increased, the electrical resistance of the sensor also increased. In comparison with various gases, for example, H_2, O_2, CO, CO_2, SO_2, and dry air, the IA-CNT-based humidity sensor exhibited high-selectivity performances. IA-CNTs also responded to heavy water (D_2O), and it was established that the humidity detection mechanism had D_2O-sensing capabilities. Further, the humidity from human out-breathing was also successfully detected by this system. In conclusion, these unique IA-CNTs exhibited potential application as gas detection materials.

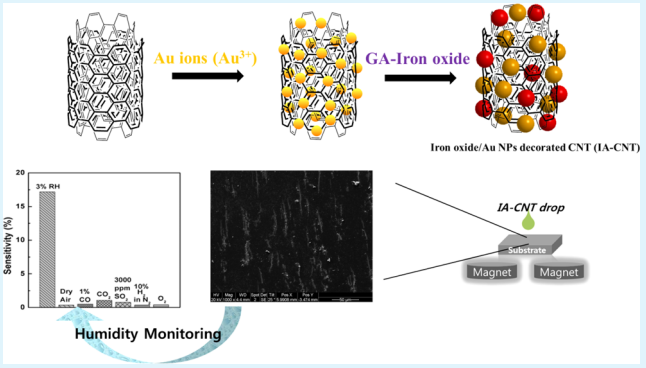

KEYWORDS: *aligned magnetoplasmonic CNT, Au/Fe_3O_4 nanoparticle-decorated CNTs, binary nanoparticle-decorated CNTs, magnetic-field alignment, oxidizable iron oxide, humidity detection*

INTRODUCTION

Humidity detectors have been widely used in various fields, ranging from human well-being to industrial processes.[1,2] They have also been extensively studied in connection with fuel-cell or battery applications. Water (H_2O) is released in fuel cells during operation, and many researchers have attempted to monitor the humidity with high selectivity against oxygen (O_2) and hydrogen (H_2).[3−5]

In general, numerous polymer-based humidity sensors have been developed because of their swelling properties in humid conditions.[6,7] The swelling effect of a polymer in a water environment can be monitored by measuring the change in its electrical conductivity and mechanical properties. In other words, humidity can be detected by translating physical and/or chemical changes into measurable electrical signals.[8−10] However, these systems face some significant challenges. First, these sensors exhibit low electroconductivity. The electrical monitoring window for these traditional humidity detectors is on the scale of megaohms. Even graphene-modified polymer hybrid structures showed similar electrical conductivity problems. Furthermore, polymer materials are easily damaged and shrink when exposed to high levels of humidity for long periods of time.[9,11,12] These deformations can cause the humidity sensing layer to become delaminated from the substrate rendering the sensor's proper utilization. Thus, many researchers have desired to develop new sensing materials to solve these critical problems.[13−16]

Recently, functionalized carbon nanotube (f-CNT)-based materials have been employed as gas- and humidity-sensing platforms because of their enhanced electrical and mechanical properties.[17−20] In particular, nanoparticle-decorated CNTs (NP-CNTs) have been highlighted because of their synergic properties, such as surface-enhanced Raman scattering, plasmonic resonance energy transfer, and magnetooptical

Received: May 4, 2015
Accepted: June 26, 2015
Published: June 26, 2015

DOI: 10.1021/acsami.5b03862
ACS Appl. Mater. Interfaces 2015, 7, 15506−15513

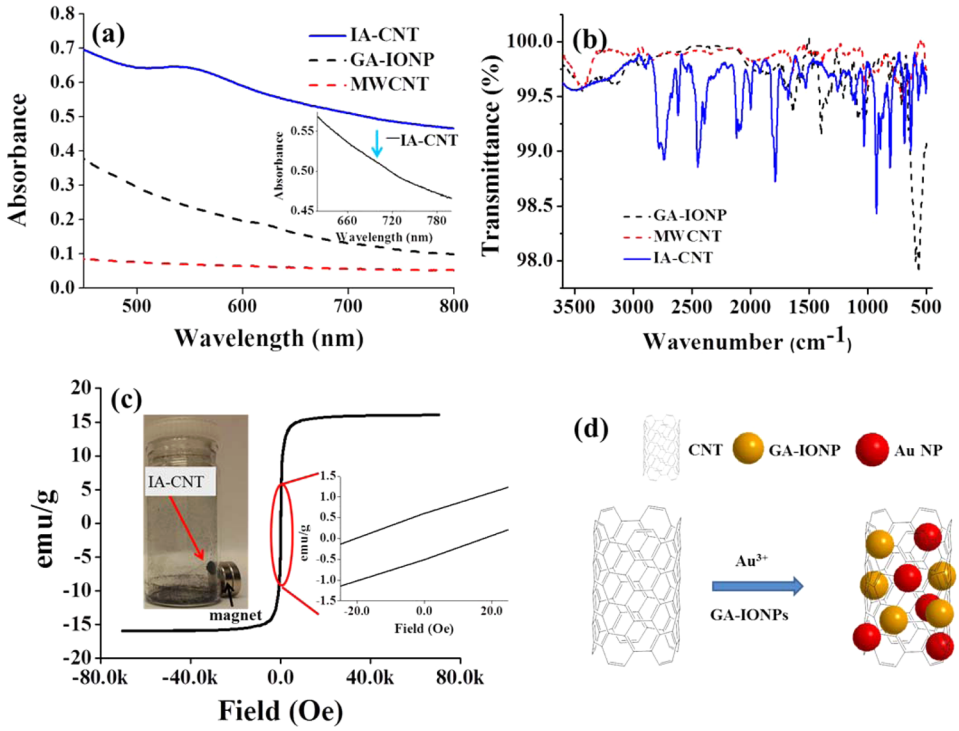

Figure 1. Physicochemical properties: (a) UV/vis spectra; (b) FT-IR spectra of IA-CNTs, GA-IONPs, and MWCNTs; (c) magnetization−hysteresis curve of IA-CNTs; (d) schematic illustration of the IA-CNT preparation (nonscalable).

effect.[21−26] These types of NP-CNTs have been applied in various fields not only in gas-sensing platforms[27−29] but also in solar cells,[30,31] secondary-ion batteries,[25,30] and nanobiomedical applications.[23,24,32]

Several methodologies have been developed to create unique NP-based f-CNTs: chemical vapor deposition,[28,33−35] chemical reduction process,[23,27] high-temperature/pressure-assisted synthesis,[36,37] electrochemical deposition,[38] soft/hard template method,[38] and DNA hybridization method.[39] Although many preparation strategies have been suggested, they are still very limited because of the complexities and difficulties in controlling these methods, and remnant byproducts from unexpected chemical reactions. A single type of NP-CNT can be prepared by using the above-mentioned methods; however, they are not often suitable for binary types of NP-CNT preparations. The synthesis of binary NP-CNTs is more complex and still faces several challenges.[40−42]

In this paper, we introduce a new process for the combination of two different NP types to be decorated on CNTs. It is a simple synthesis method for iron oxide/gold (Au) NP-decorated CNTs (IA-CNTs) in deionized (DI) water under a stirring process without exposure to any harsh conditions, chemicals, or high temperature/pressure (Figures 1d and S1 in the Supporting Information, SI). This method involved a two-step process. First, positive Au ions were attached to the surface of CNTs through electrostatic force using π electrons under the sonication process. Subsequently, gallic acid (3,4,5-trihydroxylbenzoic acid, GA)-modified iron oxide NPs (GA-IONPs) were added into the CNT/Au^{3+} solution. In this step, GA-IONPs were used as reducing agents to synthesize the Au NPs. GA possesses an antioxidant effect;[23,43] thus, GA-IONPs can play a role as oxidizable NPs. Au ions were, therefore, converted to Au NPs on the surface of CNTs using GA-IONPs, which were also attached to the surface of CNTs through $\pi-\pi$ interaction.

The physicochemical properties of nanocomposites were analyzed using ultraviolet/visible (UV/vis) spectroscopy, Fourier transform infrared (FT-IR) spectroscopy, a superconducting quantum interference device (SQUID), scanning electron microscopy (SEM), and transmission electron microscopy (TEM). Because of the magnetic properties of IA-CNTs, these nanostructures were aligned on the platinum (Pt)-based electrical circuit through an external magnetic force without a soft or hard template or other physical conditions for humidity detection purpose.

In this study, the humidity response of aligned IA-CNTs was monitored using an electrochemical impedance spectroscopy (EIS) system. The EIS system demonstrated that the aligned IA-CNT system exhibited excellent selectivity against several oxide gases, such as carbon dioxide (CO_2), carbon monoxide (CO), sulfur dioxide (SO_2), O_2, H_2, and dry synthetic air [79% nitrogen (N_2) + 21% O_2]. In addition, deuterium oxide (heavy water, D_2O, ^2H_2O) was monitored by the aligned IA-CNT system to establish any binding affinity with water vapor.

MATERIALS AND METHODS

Materials and Instruments. Chloroauric acid trihydrate ($HAuCl_4 \cdot 3H_2O$, 99.9%), GA, iron(III) chloride ($FeCl_3$), iron(II) chloride tetrahydrate ($FeCl_2 \cdot 4H_2O$), a 25% ammonium hydroxide (NH_4OH) solution, and DI water were obtained from Sigma-Aldrich (Oakville, Ontario, Canada). Multiwalled carbon nanotubes (MWCNTs) with diameters of 30−50 nm and lengths of 10−20 μm were purchased from Cheap Tubes Inc. (Cambridgeport, VT). Large-diameter (110−170 nm) MWCNTs were also obtained from Sigma-Aldrich. For IA-CNT alignment, round-type magnets (diameter of 18 mm; BrMax of 3850 G) were purchased from ABRA Electronics Inc. (Montréal, Québec, Canada). The planar interdigitated Pt electrode was purchased from Synkera (Longmont, CO).

The absorbance of GA-IONPs and IA-CNTs was measured using UV/vis spectroscopy (Cary 50, Varian Canada Inc.). The functional groups of hybrid nanostructures were monitored using FT-IR

DOI: 10.1021/acsami.5b03862
ACS Appl. Mater. Interfaces 2015, 7, 15506−15513

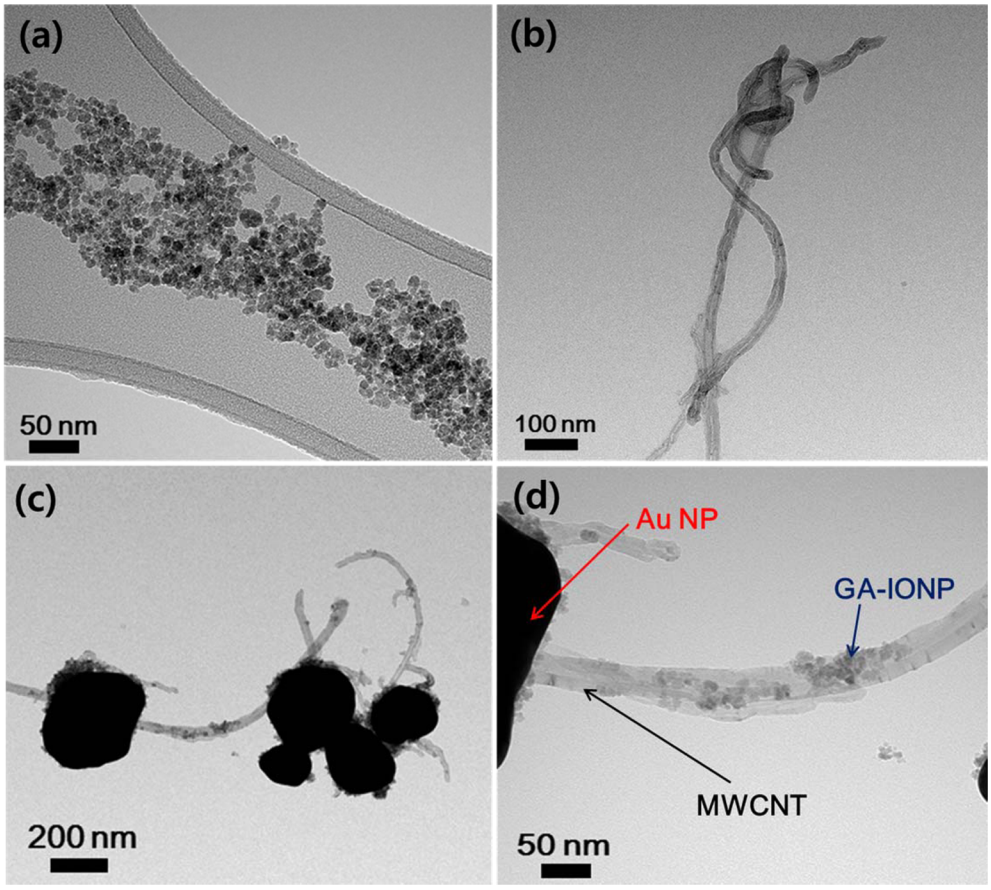

Figure 2. TEM images of (a) GA-IONPs, (b) an MWCNT, (c) an IA-CNT (low magnification), and (d) an IA-CNT (high magnification).

spectroscopy (Nexus 470 FTIR, Thermo Instruments Canada). The magnetic properties of nanostructures were analyzed using SQUID (MPMS XL, Quantum Design). The morphologies and sizes of NPs and CNTs were observed using a high-resolution transmission electron microscope (Tecnai F20, FEI, USA), a scanning electron microscope (XL30, FEI, USA), and a USB digital microscope (UDM, Microview, China). Humidity detection was performed using an EIS system (Solartron SI 1287).

Synthesis of GA-IONPs. GA-IONPs were prepared using a coprecipitation process. $FeCl_3$ (1 mmol, 0.1622 g) and $FeCl_2{\cdot}4H_2O$ (0.5 mmol, 0.0994 g) were dissolved in DI water (20 mL). Then 0.6 mL of a 25% NH_4OH solution was added to the mixture and stirred for 10 min to form iron(II,III) oxide (Fe_3O_4) NPs. Subsequently, GA powder (1.5 mmol, 0.255 g) was poured into the black Fe_3O_4 NP solution and stirred at 90 °C for 30 min. Because of the binding between GA and Fe in the GA-IONP structure, the solution color changed from black to deep violet. After stirring, GA-IONPs were purified and precipitated with excess acetone, which was finally separated out using a magnet.

Preparation of IA-CNTs. IA-CNTs were synthesized through two simple steps (Figure S1 in the SI). First, 10 mmol of $HAuCl_4{\cdot}3H_2O$ (4 mg) and 2 mg of MWCNTs were dispersed in 20 mL of DI water under sonication for 30 min. Subsequently, 1 mL of an oxidizable GA-IONP solution (1 mg/mL concentration in DI water) was dropped into the CNT/Au^{3+} mixture. After vigorous stirring for 3 h, the mixture color turned from black to dark red, indicating that IA-CNTs had been obtained. The particles were separated by magnetic force and dried in a vacuum oven.

Alignment of IA-CNTs on the Pt Electrode and Humidity Detection Test. The alignment of CNTs was desired because of the enhanced mechanical and electrical properties. A number of alignment processes have been introduced, such as a polymer-mediated injection-molding process, mechanical pulling, and electric-field-assisted alignment.[44−47] In this study, aligned IA-CNTs were formed through an external magnetic force using two magnetic bars. A total of 50 μL of an IA-CNT solution (1 mg/mL concentration) was dropped onto the Pt electrode, which was located on the two magnetic bars. In order to obtain aligned IA-CNTs, the solvent was dried at room temperature. During this process, IA-CNTs formed strawlike structures as a result of following magnetic field directions on the substrate surface.

Prototype humidity sensors were prepared by depositing IA-CNTs onto the Pt microelectrodes embedded in the alumina substrate (5 mm × 5 mm). Pt wires were kept in contact with each microelectrode in a gas-tight chamber. All sensing measurements were taken at room temperature. 1% CO (bal. in Ar), 100 ppm SO_2 (bal. in Ar), 10% H_2 (bal. in N_2), CO_2, O_2, dry synthetic air (21% O_2 in N_2) and N_2 (99.99 %) gases were purchased from Praxair Inc. (Calgary, AB, Canada). The concentration level of the gases varied in a controlled manner using a conventional gas-flow apparatus and computer-regulated mass flow controllers (MCS-100 SCCM-D/5M, 5IN).

For humidity-sensing measurements, N_2 gas was bubbled through water at various temperatures before purging into the testing chamber. The sensitivity of the sensor was monitored by the EIS system. In addition, the selectivity test was carried out for CO_2, CO, SO_2, O_2, H_2, and dry synthetic air (79% N_2 + 21% O_2). Similarly, D_2O was used instead of water by bubbling N_2 to further test the working mechanism. In this case, the IA-CNT-based sensor was able to detect 3% of D_2O, which established the binding affinity between the sensing materials and the target gases (H_2O and D_2O). The flow rate was kept constant at 100 sccm. A constant direct-current (dc) voltage of 100 mV was applied (Solartron SI 1287) to obtain an output current for both humid and corresponding gases, as noted above. The gas selectivity is defined as

$$\text{selectivity} = \frac{R_{N2} - R_G}{R_G} \times 100\% \quad (1)$$

where, R_{N2} is the electrical resistance when reference base gas N_2 is purged and R_G is the electrical resistance on the target gases (CO_2, CO,

DOI: 10.1021/acsami.5b03862
ACS Appl. Mater. Interfaces 2015, 7, 15506−15513

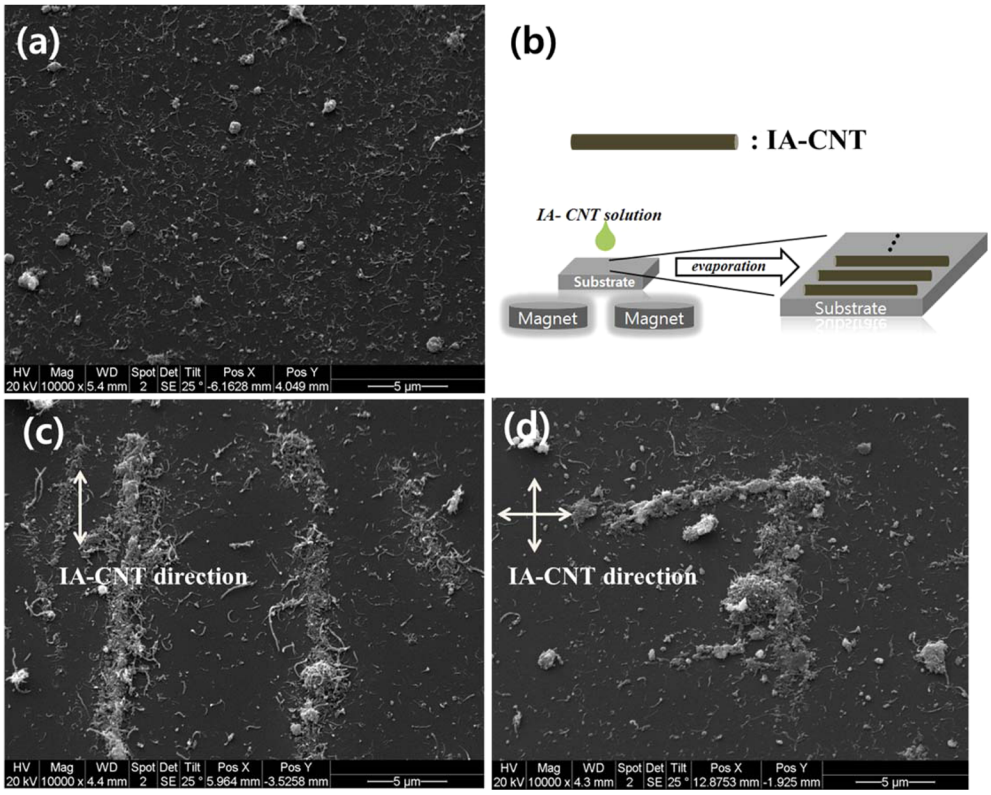

Figure 3. (a) SEM image of prealigned IA-CNTs, (b) illustration of the IA-CNT alignment process, (c) SEM image of parallel-aligned IA-CNTs, and (d) SEM image of cross-aligned IA-CNTs.

SO_2, O_2, H_2, H_2O, and D_2O) passed into the sensor chamber at various concentrations for selectivity tests.

RESULTS AND DISCUSSION

The optical absorbance was measured by UV/vis spectroscopy to confirm the surface plasmonic properties of IA-CNTs (Figure 1a). The plasmonic absorption was taken at approximately 550 nm, and the spectrum was broadened. This indicated that a large portion of Au NPs (over 50 nm) were synthesized on the MWCNT surfaces and that the size distribution of NPs was not homogeneous. In this experimental process, GA-IONPs were used as reducing agents in the preparation of Au NPs, and surfactant was not used for stabilization of the NPs. As a result, the size of the particles was not homogeneous in comparison with other strong reducing agents, such as sodium borohydride ($NaBH_4$) and hydrazine, heating, or high pressure.

This plasmonic absorption band did, however, prove that Au NPs can be successfully synthesized through only GA-IONPs without any reducing agents (such as $NaBH_4$, hydrazine, etc.), heating, high pressure, etc. In addition, the weak absorbance band (shoulder) was measured at approximately 700 nm (inset in Figure 1a). This established the longitudinal plasmon-coupling interaction that occurred between adjacent Au NPs because of the delocalized π-electron cloud on the surface of MWCNTs.[23,48] In the GA-IONP and MWCNT case, the plasmonic band was not shown. However, a weak absorption peak was analyzed in the GA-IONP spectrum at approximately 620 nm. As mentioned in the Materials and Methods section, the synthesized GA-IONPs were purple; thus, the peak was induced by binding between GA and IONPs.

The functional groups of nanomaterials were characterized by FT-IR spectroscopy (Figure 1b). The vibration band of Fe−O appeared at approximately 570 cm^{-1} in the spectra of the GA-IONPs and IA-CNTs. The carboxylic groups of IA-CNTs and GA-IONPs were measured at 1675 and 1640 cm^{-1}, respectively. The peaks at approximately 1524 cm^{-1} corresponded to the aromatic bonds of the IA-CNTs (blue spectrum in Figure 1b).

The magnetic properties of IA-CNTs were analyzed using SQUID measurements at room temperature from −80 to +80 kOe (Figure 1c). The magnetic−hysteresis relationship exhibited a nonlinear and reversible hysteresis loop (Figure 1c). From the inserted magnetization curve in Figure 1c, remanence effects are shown at approximately −0.5 and +0.6 emu/g when the applied magnetic field is zero. The coercive forces of IA-CNTs were measured to be approximately −20 and +17 Oe. The photograph in Figure 1c shows the movement of IA-CNTs with an extra magnet. The black powder indicates the presence of IA-CNTs and is located on the wall of the vial because of the magnet. The magnetization curve of the GA-IONPs is shown in Figure S2 in the SI. In this case, the remanence effects were observed at −2.0 and +2.1 emu/g, and the coercive forces were −12 and +10 Oe, indicating that the magnetization properties were maintained after the decoration reaction.

The morphologies of GA-IONPs, MWCNTs, and IA-CNTs were observed using high-resolution TEM. Figure 2a shows GA-IONPs with an approximate average size of 13 nm. These particles were well dispersed because of GA modification. In the case of organic acid binding reaction with IONPs, it is well-known that a carboxylic group of organic acid can attach to an iron oxide surface. As a result, a carboxylic group of GA can bind with iron oxide, and trihydroxyl groups can prevent aggregation between IONPs through electrical static repulsion. The trihydroxyl group of GA possesses antioxidant effects; therefore, Au ions can be converted to Au NPs using GA-IONPs.

DOI: 10.1021/acsami.5b03862
ACS Appl. Mater. Interfaces 2015, 7, 15506−15513

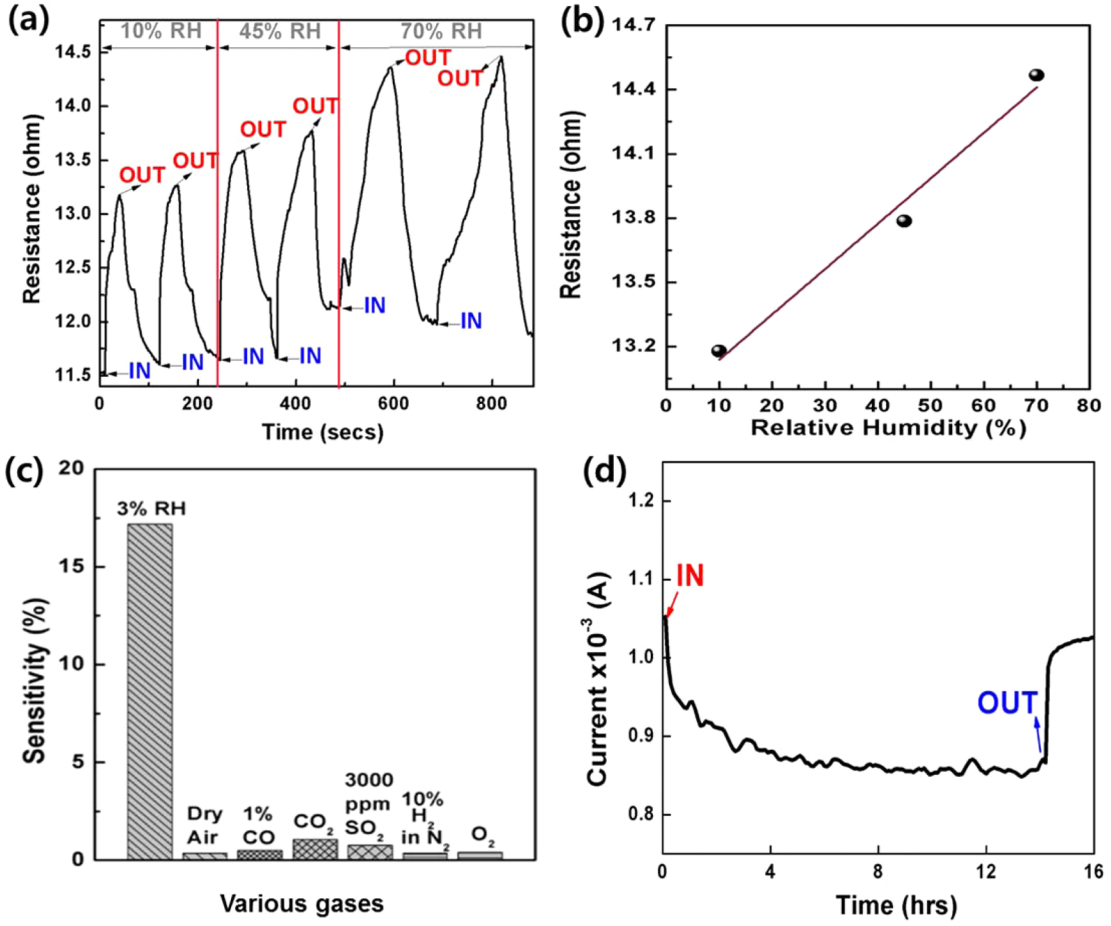

Figure 4. (a) Dynamic response of IA-CNTs under 10%, 45%, and 70% RH at 25 °C, (b) an RH-dependent sensitivity test (10%, 45%, and 70%), (c) selectivity test under the influence of various gaseous species (dry air, CO, CO_2, SO_2, H_2, and O_2) and (d) response and recovery transients of IA-CNTs under 3% RH in N_2 for long-term stability tests (~16 h) at 25 °C (pure N_2 used as the balance gas; 0.1 V applied dc voltage; 100 sccm total gas flow rate).

MWCNTs were observed in the predecoration step, showing the clean surface of the MWCNT (Figure 2b). After the two-step reactions, Au and GA-IONPs were clearly observed on the MWCNT, as seen in Figures 2c,d. The surface electrical density of Au is higher than that of IONPs; therefore, black dots indicate Au NPs, and pale-gray dots indicate IONPs. Because a surface stabilizer for Au NPs was not used in this reaction, the size of the Au NPs was slightly larger, at approximately 200 nm. In addition, GA-IONPs were well dispersed on the MWCNT and their sizes were almost the same as those of prereacted particles.

The alignment of IA-CNTs was observed through SEM and digital microscope observation. In the prealignment case, IA-CNTs were randomly dispersed on a silicon (Si) substrate (Figure 3a). To induce the alignment of IA-CNTs, a nanocomposite solution was dropped on the Si wafer surface, where it was located in the center of two magnets (Figures 3b and S3 in the SI). In this case, the magnetic field was generated between two magnets; therefore, IA-CNTs could be aligned following the external magnetic field during solvent evaporation without a soft or hard template, such as polymer or anodic aluminum oxide.

Figures 3c and S4a in the SI show parallel alignment of IA-CNTs. In this case, aligned IA-CNTs were formed in straw-bundle-like structures on the substrate because of the magnetic force interaction and surface tension during the water evaporation process. Cross-alignment of IA-CNTs was attempted using the same procedure. IA-CNTs were first aligned in parallel on the Si substrate, which was then rotated 90°, resulting in the aligned IA-CNTs being perpendicular to the magnetic field. An IA-CNT solution was then dropped on the first aligned IA-CNT layer. Cross-aligned IA-CNTs were also observed through SEM and digital microscope observation (Figures 3d and S4b in the SI).

Large-diameter IA-CNTs were also prepared and aligned using the same procedure. The alignment structures were observed through SEM (Figure S5 in the SI). These observations proved that the decoration process could occur without limitation to the CNT size and that IA-CNTs can be aligned in any direction using an external magnetic field.

Humidity detection was demonstrated by depositing aligned IA-CNTs onto a Pt electrode while utilizing an external magnetic force. In this case, the aligned IA-CNTs were used as a humidity-sensing channel. The EIS system monitored IA-CNTs having 10%, 45%, and 70% of relative humidity (RH) contents for dynamic responses. The resistance of IA-CNTs increased as the water vapor was introduced into the sensing channel. After IA-CNT channels were exposed to moisture, water molecules were absorbed on the surfaces of IA-CNTs. During this process, a charge-transfer incident took place because of the difference in the electrical potential between water molecules and IA-CNTs.[49,50] In turn, this showed that the electrical conductivity could change under the humid environment (Figure 4a). Furthermore, electrical conductivity variation could occur by the difference in induced charge transfer of various humid contents. In contrast, when water vapor was removed, the

DOI: 10.1021/acsami.5b03862
ACS Appl. Mater. Interfaces 2015, 7, 15506−15513

resistance tended to revert back to its initial state. The response and recovery transients were consistent with similar subsequent cycles, thus exhibiting high reproducibility in various conditions.

Depending on the humidity contents, the response of IA-CNTs varied (Figure 4b). High RH induced high resistance of IA-CNTs. In the 10% RH case, the resistance of IA-CNTs was approximately 13.2 Ω, and the resistances reached about 13.7 and 14.7 Ω at 45 and 70% RH, respectively. Especially, compared with polymeric or metal oxide based humidity-sensing materials, this hybrid structure showed high electrical conductivity, and it established that the accuracy of detection might be improved with other sensing materials.

The selectivity test was applied to various gases, such as CO_2, CO, SO_2, O_2, H_2, and dry synthetic air (Figure S6 in the SI). All of the gases with various concentrations were exposed to the IA-CNT gas-sensing channel. The selectivity of the IA-CNT-based humidity sensor was expressed using eq 1. Figure 4c shows that the selectivity was very high for humid gas obtained by bubbling N_2 through a water bubbler at room temperature (i.e., 3% RH). A significant change in the current (at 0.1 V) was not observed in the cases of other gaseous species [CO_2, CO, dry synthetic air (21% O_2 in N_2), H_2, and SO_2] that passed through the same gas-tight cell at various concentrations under the same conditions (25 °C and total gas flow of 100 sccm). The other gases were also identified in presence of N2 as diluting gas.

The selectivity of the IA-CNT sample was calculated using various gaseous species by comparing the changes in the resistance of the material (at different ppm levels), i.e., sensitivity according to eq 1. As shown in Figure 4c, the aligned channel responded to H_2O vapor with a sensitivity of approximately 17%. The detection test was carried out for a long period, taking more than 15 h, with 3% RH (Figure 4d) at room temperature. In this case, the removal of 3% RH generated a rapid recovery signal (electric current), which was close to the original value ($\sim 1.05 \times 10^{-3}$ A) before the sample came into contact with humidity.

Moreover, each component of the hybrid structure was used as a sensing channel material for the control test. In Figure S7 in the SI, bare CNT could capture moisture, but its dynamic sensing ability and electrical conductivity were very low comparing to that of an IA-CNT. These factors were closely related with sensing accuracy. Furthermore, in the case of Au-CNT, the electrical conductivity improved more than it did for bare CNT; however, the sensing ability decreased significantly. Also, IO-CNT could detect the moisture, but its conductivity and sensitivity were worse than those of the bare CNT case. Therefore, all hybrid nanostructures can induce a synergic effect, which may lead to high conductivity as well as fast response and recovery. These results are very promising and may lead to the further development of the IA-CNT sensor into a highly selective and durable humidity sensor.

In the D_2O (^2H_2O) case, the current of the sensing channel decreased by less than half the scale of the H_2O, indicating that the behavior of the interaction between IA-CNTs and normal water and heavy water differs. The interaction between water molecules and IA-CNTs is still not clear, and the system should be studied further in this respect.

Nonetheless, our study established that a hydrogen type of water can be distinguished by the IA-CNT sensing channel (Figure 5). One of the humidity detection mechanism hypotheses on IA-CNTs is related to hydrogen bonding.[51,52] In the FT-IR spectrum of IA-CNTs (in Figure 1b), two OH vibrations were observed around 3250 cm^{-1} (weak) and 3514 cm^{-1} (strong) in iron oxide and CNTs. This part of the IA-CNTs

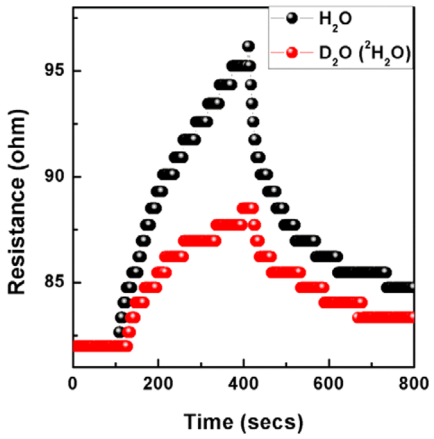

Figure 5. Response and recovery behavior of IA-CNTs under the influence of 3% H_2O and D_2O (^2H_2O) (applied voltage = 0.1 V; total flow rate = 100 sccm).

can induce hydrogen bonding with H_2O and D_2O. Furthermore, the hydrogen-bonding force between H_2O and D_2O could be different using IA-CNTs, so they may be distinguishable with this system.[53−55] Similar to other gases (except 3% RH), H_2 gas did not show significant changes upon exposure to IA-CNTs (Figure 4c). This result and further investigations may lead us to find the potential mechanism of IA-CNTs' sensing behavior.

The humidity in human outbreathing was successfully detected using the IA-CNT-sensing system. In this case, outbreathing was blown into the IA-CNT channel (video S1 in the SI). Interestingly, the electrical resistance dramatically changed by blowing breath out into the IA-CNT-coated sensor (Figure 6 and video S1 in the SI). In the video, the response is

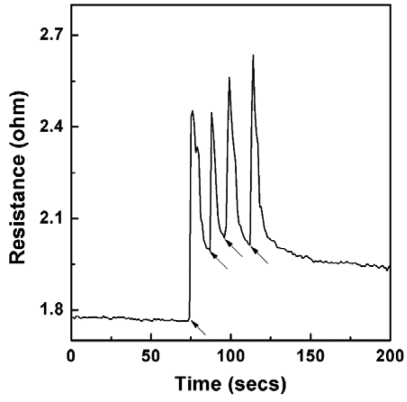

Figure 6. Humidity detection through human breathing.

shown in terms of the current (applied voltage of 0.1 V), whereas it is shown in terms of resistance values in Figure 6. Breathing out is represented by arrows, where a fast response can be observed. In addition, a fast recovery can also be seen when breathing out ceased. As was previously mentioned, water molecules were absorbed on IA-CNTs via the formation of hydrogen bonding. In the case of an open chamber without carrier gas assistance, water molecules could not be removed completely because of the strong hydrogen-bonding-induced interaction force. However, for the case of a closed chamber, water molecules could be removed from the surfaces of IA-CNTs by a continuous flowing force of carrier gas (N_2 gas), allowing the sensor to revert back to its initial value. This result showed that IA-CNTs could

DOI: 10.1021/acsami.5b03862
ACS Appl. Mater. Interfaces 2015, 7, 15506−15513

potentially be applied as miniaturized humidity sensors at room temperature with fast response, high sensitivity, and high selectivity.

CONCLUSION

IA-CNTs were successfully synthesized using an oxidizable GA-IONP-assisted synthesis method, which does not require high temperature, high pressure, or harsh reducing agents. This hybrid material was synthesized through two simple steps in DI water. IA-CNTs were aligned on the substrate using an external magnetic field without a hard or soft template. Crossed structures of IA-CNTs were formed in layers through layer deposition on the substrate.

In order to perform humidity-sensing applications, IA-CNTs were deposited on the Pt-based electrode to monitor the electrical changes. Interestingly, f-CNTs did not respond to various gases, such as CO_2, CO, SO_2, and dry air (79% N_2 and 21% O_2 mixture). However, they did show excellent sensing selectivity with humidity. Thus, these hybrid CNTs possess high potential as humidity-sensing platforms in nanoelectronic fields through a simple alignment process.

ASSOCIATED CONTENT

Supporting Information

Schematic illustrations for the preparation of IA-CNTs, hysteresis curve of GA-IONPs, photograph of the alignment process, digital microscopic image of aligned IA-CNTs, SEM images of large-sized IA-CNTs, and detection selectivity data of IA-CNTs, and a video clip showing the monitoring of humidity from human out-breathing using an IA-CNT sensing system. The Supporting Information is available free of charge on the ACS Publications website at DOI: 10.1021/acsami.5b03862.

AUTHOR INFORMATION

Corresponding Authors

*E-mail: jaewook.lee@ucalgary.ca.
*E-mail: sipark@ucalgary.ca.

Notes

The authors declare no competing financial interest.

ACKNOWLEDGMENTS

The authors are grateful to Dr. Simon Trudel for the SQUID measurements. The authors acknowledge support of the Natural Sciences and Engineering Research Council of Canada (NSERC), Alberta Innovates Technology Future (AITF), Korea Carbon Capture and Sequestration R&D Center (KCRC), and Korea Institute of Geoscience and Mineral Resources (KIGAM). This research was also supported by an Eyes High research fellowship from the University of Calgary.

REFERENCES

(1) Bi, H. C.; Yin, K. B.; Xie, X.; Ji, J.; Wan, S.; Sun, L. T.; Terrones, M.; Dresselhaus, M. S. Ultrahigh Humidity Sensitivity of Graphene Oxide. *Sci. Rep.* **2013**, *3*, 2714:1−2714:7.

(2) Saha, A.; Tanaka, Y.; Han, Y.; Bastiaansen, C. M. W.; Broer, D. J.; Sijbesma, R. P. Irreversible Visual Sensing of Humidity Using a Cholesteric Liquid Crystal. *Chem. Commun.* **2012**, *48* (38), 4579−4581.

(3) Inman, K.; Wang, X. Detection of Liquid Water in the Flow Channels of PEM Fuel Cell Using an Optical Sensor. *Int. J. Hydrogen Energy* **2014**, *39* (34), 19691−19700.

(4) Bell, S.; Hinds, G.; de Podesta, M.; Stevens, M.; Wilkinson, J. Humidity, Pressure, and Temperature Measurements in an Interdigitated-Flow PEM Hydrogen Fuel Cell. *Int. J. Thermophys.* **2012**, *33* (8−9), 1583−1594.

(5) Morris, D. R. P.; Liu, S. P.; Villegas Gonzalez, D.; Gostick, J. T. Effect of Water Sorption on the Electronic Conductivity of Porous Polymer Electrolyte Membrane Fuel Cell Catalyst Layers. *ACS Appl. Mater. Interfaces* **2014**, *6* (21), 18609−18618.

(6) Wang, X. F.; Ding, B.; Yu, J. Y.; Wang, M. R. Highly Sensitive Humidity Sensors Based on Electro-Spinning/Netting a Polyamide 6 Nano-Fiber/Net Modified by Polyethyleneimine. *J. Mater. Chem.* **2011**, *21* (40), 16231−16238.

(7) Zhang, J.; Zhong, J.; Fang, Y. F.; Wang, J.; Huang, G. S.; Cui, X. G.; Mei, Y. F. Roll Up Polymer/Oxide/Polymer Nanomembranes as a Hybrid Optical Microcavity for Humidity Sensing. *Nanoscale* **2014**, *6* (22), 13646−13650.

(8) Su, P. G.; Wang, C. S. Novel Flexible Resistive-Type Humidity Sensor. *Sens. Actuators, B* **2007**, *123* (2), 1071−1076.

(9) Liu, K.; Li, Y.; Zhang, G. Q.; Lv, X.; Yang, M. J. The Effect of Humidity on the Electrical Behavior of a Cationic Conjugated Polyelectrolyte Based on Poly(phenylene vinylene). *Sens. Actuators, B* **2009**, *135* (2), 597−602.

(10) Su, P. G.; Tseng, J. Y.; Huang, Y. C.; Pan, H. H.; Li, P. C. Novel Fully Transparent and Flexible Humidity Sensor. *Sens. Actuators, B* **2009**, *137* (2), 496−500.

(11) Chen, C.; Fuller, T. F. The Effect of Humidity on the Degradation of Nafion (R) Membrane. *Polym. Degrad. Stab.* **2009**, *94* (9), 1436−1447.

(12) Su, P. G.; Chiou, C. F. Electrical and Humidity-Sensing Properties of Reduced Graphene Oxide Thin Film Fabricated by Layer-by-Layer with Covalent Anchoring on Flexible Substrate. *Sens. Actuators, B* **2014**, *200*, 9−18.

(13) Zhang, S. L.; Jung, H.; Huh, J. S.; Yu, J. B.; Yang, W. C. Efficient Exfoliation of MoS2 with Volatile Solvents and Their Application for Humidity Sensor. *J. Nanosci. Nanotechnol.* **2014**, *14* (11), 8518−8522.

(14) Xie, W. Y.; Liu, B.; Xiao, S. H.; Li, H.; Wang, Y. R.; Cai, D. P.; Wang, D. D.; Wang, L. L.; Liu, Y.; Li, Q. H.; Wang, T. H. High Performance Humidity Sensors Based on CeO_2 Nanoparticles. *Sens. Actuators, B* **2015**, *215*, 125−132.

(15) Tang, Y. L.; Li, Z. J.; Ma, J. Y.; Wang, L.; Yang, J.; Du, B.; Yu, Q. K.; Zu, X. T. Highly Sensitive Surface Acoustic Wave (SAW) Humidity Sensors Based on Sol-Gel SiO_2 Films: Investigations on the Sensing Property and Mechanism. *Sens. Actuators, B* **2015**, *215*, 283−291.

(16) Feng, X. Y.; Chen, W. F.; Yan, L. F. Free-Standing Dried Foam Films of Graphene Oxide for Humidity Sensing. *Sens. Actuators, B* **2015**, *215*, 316−322.

(17) Bekyarova, E.; Kalinina, I.; Sun, X. B.; Shastry, T.; Worsley, K.; Chi, X. L.; Itkis, M. E.; Haddon, R. C. Chemically Engineered Single-Walled Carbon Nanotube Materials for the Electronic Detection of Hydrogen Chloride. *Adv. Mater.* **2010**, *22* (7), 848−852.

(18) Hines, D.; Rummeli, M. H.; Adebimpe, D.; Akins, D. L. High-Yield Photolytic Generation of Brominated Single-Walled Carbon Nanotubes and Their Application for Gas Sensing. *Chem. Commun.* **2014**, *50* (78), 11568−11571.

(19) Kybert, N. J.; Lerner, M. B.; Yodh, J. S.; Preti, G.; Johnson, A. T. C. Differentiation of Complex Vapor Mixtures Using Versatile DNA-Carbon Nanotube Chemical Sensor Arrays. *ACS Nano* **2013**, *7* (3), 2800−2807.

(20) Schnorr, J. M.; van der Zwaag, D.; Walish, J. J.; Weizmann, Y.; Swager, T. M. Sensory Arrays of Covalently Functionalized Single-Walled Carbon Nanotubes for Explosive Detection. *Adv. Funct. Mater.* **2013**, *23* (42), 5285−5291.

(21) Wang, X. J.; Wang, C.; Cheng, L.; Lee, S. T.; Liu, Z. Noble Metal Coated Single-Walled Carbon Nanotubes for Applications in Surface Enhanced Raman Scattering Imaging and Photothermal Therapy. *J. Am. Chem. Soc.* **2012**, *134* (17), 7414−7422.

(22) Panczyk, T.; Drach, M.; Szabelski, P.; Jagusiak, A. Magnetic Anisotropy Effects on the Behavior of a Carbon Nanotube Functionalized by Magnetic Nanoparticles Under External Magnetic Fields. *J. Phys. Chem. C* **2012**, *116* (49), 26091−26101.

DOI: 10.1021/acsami.5b03862
ACS Appl. Mater. Interfaces 2015, 7, 15506−15513

(23) Lee, J.; Ahmed, S. R.; Oh, S.; Kim, J.; Suzuki, T.; Parmar, K.; Park, S. S.; Lee, J.; Park, E. Y. A Plasmon-Assisted Fluoro-Immunoassay Using Gold Nanoparticle-Decorated Carbon Nanotubes for Monitoring the Influenza Virus. *Biosens. Bioelectron.* **2015**, *64*, 311−317.
(24) Gao, C.; Guo, Z.; Liu, J. H.; Huang, X. J. The New Age of Carbon Nanotubes: An Updated Review of Functionalized Carbon Nanotubes in Electrochemical Sensors. *Nanoscale* **2012**, *4* (6), 1948−1963.
(25) Tucek, J.; Kemp, K. C.; Kim, K. S.; Zboril, R. Iron-Oxide-Supported Nanocarbon in Lithium-Ion Batteries, Medical, Catalytic, and Environmental Applications. *ACS Nano* **2014**, *8* (8), 7571−7612.
(26) Mazloumi, M.; Shadmehr, S.; Rangom, Y.; Nazar, L. F.; Tang, X. W. Fabrication of Three-Dimensional Carbon Nanotube and Metal Oxide Hybrid Mesoporous Architectures. *ACS Nano* **2013**, *7* (5), 4281−4288.
(27) Popa, A.; Li, J.; Samia, A. C. S. Hybrid Platinum Nanobox/Carbon Nanotube Composites for Ultrasensitive Gas Sensing. *Small* **2013**, *9* (23), 3928−3933.
(28) Zanolli, Z.; Leghrib, R.; Felten, A.; Pireaux, J. J.; Llobet, E.; Charlier, J. C. Gas Sensing with Au-Decorated Carbon Nanotubes. *ACS Nano* **2011**, *5* (6), 4592−4599.
(29) Abdelhalim, A.; Abdellah, A.; Scarpa, G.; Lugli, P. Metallic Nanoparticles Functionalizing Carbon Nanotube Networks for Gas Sensing Applications. *Nanotechnology* **2014**, *25* (5), 055208:1−055208:10.
(30) Maiti, U. N.; Lee, W. J.; Lee, J. M.; Oh, Y.; Kim, J. Y.; Kim, J. E.; Shim, J.; Han, T. H.; Kim, S. O. 25th Anniversary Article: Chemically Modified/Doped Carbon Nanotubes & Graphene for Optimized Nanostructures & Nanodevices. *Adv. Mater.* **2014**, *26* (1), 40−67.
(31) Azoz, S.; Jiang, J.; Keskar, G.; McEnally, C.; Alkas, A.; Ren, F.; Marinkovic, N.; Haller, G. L.; Ismail-Beigi, S.; Pfefferle, L. D. Mechanism for Strong Binding of CdSe Quantum Dots to Multiwall Carbon Nanotubes for Solar Energy Harvesting. *Nanoscale* **2013**, *5* (15), 6893−6900.
(32) Lee, J.; Kim, J.; Ahmed, S. R.; Zhou, H.; Kim, J. M.; Lee, J. Plasmon-Induced Photoluminescence Immunoassay for Tuberculosis Monitoring Using Gold-Nanoparticle-Decorated Graphene. *ACS Appl. Mater. Interfaces* **2014**, *6* (23), 21380−21388.
(33) Tucek, J.; Kemp, K. C.; Kim, K. S.; Zboril, R. Iron-Oxide-Supported Nanocarbon in Lithium-Ion Batteries, Medical, Catalytic, and Environmental Applications. *ACS Nano* **2014**, *8* (8), 7571−7612.
(34) Liang, C. H.; Xia, W.; van den Berg, M.; Wang, Y. M.; Soltani-Ahmadi, H.; Schluter, O.; Fischer, R. A.; Muhler, M. Synthesis and Catalytic Performance of Pd Nanoparticle/Functionalized CNF Composites by a Two-Step Chemical Vapor Deposition of Pd(allyl)-(Cp) Precursor. *Chem. Mater.* **2009**, *21* (12), 2360−2366.
(35) Sharma, H.; Agarwal, D. C.; Shukla, A. K.; Avasthi, D. K.; Vankar, V. D. Surface-Enhanced Raman Scattering and Fluorescence Emission of Gold Nanoparticle-Multiwalled Carbon Nanotube Hybrids. *J. Raman Spectrosc.* **2013**, *44* (1), 12−20.
(36) Georgakilas, V.; Gournis, D.; Tzitzios, V.; Pasquato, L.; Guldi, D. M.; Prato, M. Decorating Carbon Nanotubes with Metal or Semiconductor Nanoparticles. *J. Mater. Chem.* **2007**, *17* (26), 2679−2694.
(37) Zheng, S. F.; Hu, J. S.; Zhong, L. S.; Wan, L. J.; Song, W. G. In Situ One-Step Method for Preparing Carbon Nanotubes and Pt Composite Catalysts and Their Performance for Methanol Oxidation. *J. Phys. Chem. C* **2007**, *111* (30), 11174−11179.
(38) Peng, X. H.; Chen, J. Y.; Misewich, J. A.; Wong, S. S. Carbon Nanotube-Nanocrystal Heterostructures. *Chem. Soc. Rev.* **2009**, *38* (4), 1076−1098.
(39) Su, H. C.; Zhang, M. L.; Bosze, W.; Lim, J.-H.; Myung, N. V. Metal Nanoparticles and DNA co-Functionalized Single-Walled Carbon Nanotube Gas Sensors. *Nanotechnology* **2013**, *24* (50), 505502:1−505502:11.
(40) Yang, P.; Jin, S. Y.; Xu, Q. Z.; Yu, S. H. Decorating PtCo Bimetallic Alloy Nanoparticles on Graphene as Sensors for Glucose Detection by Catalyzing Luminol Chemiluminescence. *Small* **2013**, *9* (2), 199−204.
(41) Zeng, T.; Zhang, X. L.; Ma, Y. R.; Niu, H. Y.; Cai, Y. Q. A Novel Fe_3O_4-Graphene-Au Multifunctional Nanocomposite: Green Synthesis and Catalytic Application. *J. Mater. Chem.* **2012**, *22* (35), 18658−18663.
(42) Guo, S. J.; Zhang, S.; Wu, L. H.; Sun, S. H. Co/CoO Nanoparticles Assembled on Graphene for Electrochemical Reduction of Oxygen. *Angew. Chem., Int. Ed.* **2012**, *51* (47), 11770−11773.
(43) Lee, J.; Kim, H. Y.; Zhou, H.; Hwang, S.; Koh, K.; Han, D. W.; Lee, J. Green Synthesis of Phytochemical-Stabilized Au Nanoparticles under Ambient Conditions and Their Biocompatibility and Antioxidative Activity. *J. Mater. Chem.* **2011**, *21* (35), 13316−13326.
(44) Arjmand, M.; Mahmoodi, M.; Gelves, G. A.; Park, S.; Sundararaj, U. Electrical and Electromagnetic Interference Shielding Properties of Flow-Induced Oriented Carbon Nanotubes in Polycarbonate. *Carbon* **2011**, *49* (11), 3430−3440.
(45) Parmar, K.; Mahmoodi, M.; Park, C.; Park, S. S. Effect of CNT Alignment on the Strain Sensing Capability of Carbon Nanotube Composites. *Smart Mater. Struct.* **2013**, *22* (7), 075006:1−075006:12.
(46) Park, C.; Wilkinson, J.; Banda, S.; Ounaies, Z.; Wise, K. E.; Sauti, G.; Lillehei, P. T.; Harrison, J. S. Aligned Single-Wall Carbon Nanotube Polymer Composites using an Electric Field. *J. Polym. Sci., Part B: Polym. Phys.* **2006**, *44* (12), 1751−1762.
(47) Allen, R.; Pan, L. J.; Fuller, G. G.; Bao, Z. A. Using In-Situ Polymerization of Conductive Polymers to Enhance the Electrical Properties of Solution-Processed Carbon Nanotube Films and Fibers. *ACS Appl. Mater. Interfaces* **2014**, *6* (13), 9966−9974.
(48) Lee, J.; Zhou, H.; Lee, J. Small Molecule Induced Self-Assembly of Au Nanoparticles. *J. Mater. Chem.* **2011**, *21* (42), 16935−16942.
(49) Paul, A.; Bhattacharya, B.; Bhattacharyya, T. K. Electric-Field Assisted Desorption of Water Molecules in DNA Functionalized CNT Network. *IEEE Sens. J.* **2015**, *15* (5), 2947−2950.
(50) Jung, D.; Kim, J.; Lee, G. S. Enhanced Humidity-Sensing Response of Metal Oxide Coated Carbon Nanotube. *Sens. Actuators, A* **2015**, *223*, 11−17.
(51) Kendelewicz, T.; Liu, P.; Doyle, C. S.; Brown, G. E.; Nelson, E. J.; Chambers, S. A. Reaction of Water with the (100) and (111) Surfaces of Fe_3O_4. *Surf. Sci.* **2000**, *453* (1−3), 32−46.
(52) Watts, P. C. P.; Mureau, N.; Tang, Z.; Miyajima, Y.; Carey, J. D.; Silva, S. R. P. The Importance of Oxygen-Containing Defects on Carbon Nanotubes for the Detection of Polar and Non-Polar Vapours through Hydrogen Bond Formation. *Nanotechnology* **2007**, *18* (17), 175701:1−175701:6.
(53) Parkinson, G. S.; Kim, Y. K.; Dohnalek, Z.; Smith, R. S.; Kay, B. D. Reactivity of Fe-0 Atoms and Clusters with D_2O over FeO(111). *J. Phys. Chem. C* **2009**, *113* (12), 4960−4969.
(54) Cutting, R. S.; Muryn, C. A.; Vaughan, D. J.; Thornton, G. Substrate-Termination and H_2O-Coverage Dependent Dissociation of H_2O on Fe_3O_4(111). *Surf. Sci.* **2008**, *602* (6), 1155−1165.
(55) Takeda, M.; Miyanoiri, Y.; Terauchi, T.; Yang, C. J.; Kainosho, M. Use of H/D Isotope Effects to Gather Information about Hydrogen Bonding and Hydrogen Exchange Rates. *J. Magn. Reson.* **2014**, *241*, 148−154.

DOI: 10.1021/acsami.5b03862
ACS Appl. Mater. Interfaces 2015, 7, 15506−15513